**Applied Energy Symposium 2021: Low carbon cities and urban energy systems**
**September 4-8, 2021, Matsue, Japan**
**Paper ID: 51**

# Numerical study on effects of sudden heat flux increase on flow pattern in straight microchannel for CPV cooling

Li Tongling[1], Yu Hao[1], Li Wenfei[1], Zhuang Jiaojiao[1], Meng Shuangshuang[1], Mao Ning[1,2*]

1 Department of Gas Engineering, College of Pipeline and Civil Engineering, China University of Petroleum (East China), China

2 Institute of Industrial Science, The University of Tokyo, Tokyo, Japan

## ABSTRACT

Microchannel boiling was used for cooling concentrated photovoltaic (CPV) due to its promising heat transfer performance, to maintain the normal operating of CPV at a high efficiency. However, fluctuating and non-uniform heat fluxes of CPVs may lead to deterioration of flow boiling and heat transfer of microchannel, and then reduce the heat dissipation performance of CPV, and lead to damage of solar cells. To improve this key point, a rectangular straight microchannel with deionized (DI) water boiling was numerically simulated using VOF method, four sudden heat flux increase levels were set: 97.96, 199.64, 284.54 and 580 kW/m$^2$. The effects of sudden heat flux increase on the two-phase flow pattern was studied. It was found the higher heat flux increase advanced the generation of water vapor phase and transition. The water vapor volume fraction was instantaneously increased and easily moved to instability under heat flux increase of 580 kW/m$^2$.

**Keywords:** CPV cooling, microchannel flow boiling, flow pattern, sudden heat flux increase, numerical study

## NONMENCLATURE

| | |
|---|---|
| *Abbreviations* | |
| CPV | Concentrated photovoltaic |
| VOF | Volume of fluid |
| *Symbols* | |
| $T$ | Temperature (℃) |
| $\rho$ | Density (kg/m$^3$) |
| $\Delta p$ | Pressure drop (Pa) |

## 1. INTRODUCTION

In recent years, concentrated photovoltaic (CPV) technology has attracted increasing attentions, due to its benefits in advancing the photoelectric efficiency of PV system and reducing costs [1]. However, the high radiation intensity leads to significantly increase in PV temperature, which deteriorates the photoelectric efficiency, or even damages the PV cells. So, necessary heat dissipation is needed for normal maintaining of the CPVs. For CPVs with higher than 150 suns of solar radiation intensity, a much higher heat transfer coefficient above 104 W/K/m$^2$ was required [2], to control the temperature of PV cells, which should be realized through effective cooling technology. microchannel flow boiling has attracted continuously increasing attentions in recent years and became one of the most promising solution to advance cooling of high-flux equipment [3], attributing to higher surface to volume ratio, higher heat transfer, small scale and high latent heat transfer. A number of studies have been carried out on microchannel used for cooling CPV previously [4,5,6], which indicate the effective cooling performance.

Although the microchannel boiling shows excellent performance in reducing solar cell temperature and improving efficiency of solar cell or PVT module, after a detailed review on Microchannel cooling of concentrator photovoltaics, Gilmore et al. [7] pointed out that the fluctuating and non-uniform heat fluxes of CPVs may lead to challenges to microchannel boiling for cooling CPV.

Therefore, it's mandatory to study the effects of dynamic heat flux, especially sudden increase in heat flux, on flow boiling characteristics in microchannel. To

*Corresponding author: Mao Ning
Selection and peer-review under responsibility of the scientific committee of CUE2021

understand the fundamental of fluid mechanism, a straight single microchannel with rectangular cross section was designed, and a numerical study was carried out on the two-phase flow pattern inside the channel

## 2. METHODOLOGY

### *2.1 Physical model*

The physical model of the microchannel has the same structure as the previous experimental [8], as shown in Fig. 1. The rectangular microchannel is placed horizontally, and copper was used as material. The size of the model is 0.4×0.4×58mm. Mesh was generated, as shown in Fig. 1.

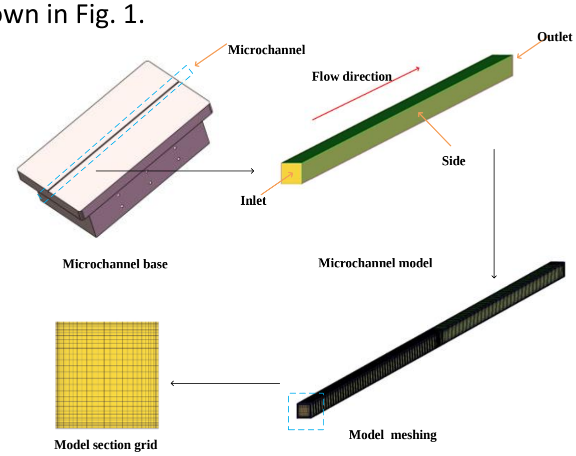


Fig. 1 Rectangular microchannel physical model and meshing

ANSYS FLUENT 17.0 is used for simulating flow boiling in microchannel. Copper is used as the solid material of the microchannel. The working fluid in the microchannel is water liquid and water vapor. In order to ensure the accuracy of the simulation, the change of the physical parameters caused by the temperature cannot be ignored. Equations of the physical parameters of water liquid depending on temperature were used.

### *2.2 Numerical method*

The main governing equations are as follows:

Equation of continuity:

$$\frac{\partial \rho}{\partial t}+\frac{\partial\left(\rho u_x\right)}{\partial x}+\frac{\partial\left(\rho u_y\right)}{\partial y}+\frac{\partial\left(\rho u_z\right)}{\partial z}=0 \tag{1}$$

The tracking of the interface between phases is accomplished by solving the continuity equation for the volume fraction of one (or more) phases based on the VOF model. The continuity equation for the volume fraction of the multiphase is shown below

$$\frac{1}{\rho_q}\left[\frac{\partial}{\partial t}\left(\partial_q \rho_q\right)+\nabla \cdot\left(\alpha_q \rho_q \vec{v}_q\right)=S_{\partial q}+\sum_{p=1}^{n} \dot{m}_{pq}-\dot{m}_{qp}\right] \tag{2}$$

$\dot{m}_{qp}$ is the mass transfer from phase q to phase p, and $\dot{m}_{pq}$ is the mass transfer from phase p to phase q.

Momentum conservation equation:

$$\frac{\partial}{\partial t}(\rho \vec{v})+\nabla \cdot(\rho \vec{v} \vec{v})=-\nabla p+\nabla \cdot\left[\mu\left(\nabla \vec{v}+\nabla \vec{v}^{T}\right)\right]+\rho \vec{g}+\vec{F} \tag{3}$$

Energy conservation equation:

$$\frac{\partial}{\partial t}(\rho E)+\nabla \cdot(\vec{v}(\rho E+p))=\nabla \cdot\left(k_{eff} \nabla T\right)+S_h \tag{4}$$

The VOF model regards energy *E* and temperature *T* as mass average variables.

Mass transfer equation in evaporation and condensation model:

If $T \geq T_{sat}$,

$$\dot{m}_{ev}=0.1 \times \alpha_l \rho_l \frac{(T-T_{sat})}{T_{sat}} \tag{5}$$

If $T \leq T_{sat}$,

$$\dot{m}_{ev}=0.1 \times \alpha_v \rho_v \frac{(T-T_{sat})}{T_{sat}} \tag{6}$$

### *2.3 Boundary conditions*

(1) The inlet of the microchannel is set as the velocity inlet, with inlet velocity of 0.677 m/s, and inlet temperature of 323.15 K. The volume fraction of water vapor at inlet is set to be 0;

(2) The outlet of the microchannel is set as the pressure outlet;

(3) The constant heat flux was applied to the bottom wall and side walls. And the top wall is considered as adiabatic.

### *2.4 Solving method*

The Volume of Fluid (VOF) method, phase change model and surface tension model are considered in the simulation. The advantage of the VOF model is that it can track the volume fraction of two or more incompatible fluids in the entire region. The body force formulations were solved in implicit methods. The evaporation-condensation mechanism is used for mass transfer. The value of surface tension coefficient is 0.056 N/m between water liquid and water vapor. The scheme of pressure and velocity coupling is coupled. This solver offers some advantages over the pressure-based segregated algorithm. PRESTO! (Pressure Staggering Option) is used for pressure and Second Order Upwind is used for energy and momentum equation solution. The governing equations are solved by the Gauss-Seidel iterative solver and the normalized residual of the equations is limited to below $10^{-5}$. The time step size is set to be $10^{-6}$s.

### *2.5 Mesh dependence and validation*

The number of grids will affect the results of numerical calculations. Therefore, it is necessary to verify the grid independence to ensure the accuracy of the results with an appropriate number of grids. The calculation condition for grid independence verification is: the inlet velocity is 0.225m/s, and the heat flux on the bottom and left and right sides is 16kW/m$^2$. The number of grids are 675000, 810000, 1.08 million, 1.44 million, and 1.92 million respectively. The variation of the pressure drop between the inlet and outlet of the microchannel with the number of grids is shown in Fig. 5. And the difference between the pressure drop when the grid number is 1.44 million and 1.92 million is less than 1.5%, which meets the requirements of grid independence verification. Therefore, the grid of 1.44 million was used for the following study.

In order to verify the accuracy of the CFD model, the simulated data was compared with experimental data, as shown in Fig. 3. It's shown that with the increase of heat flux, the variation trend of the pressure drop is the same as that of the experiment, and the difference is much lower. Therefore, it can be considered that the numerical calculation results are in good agreement with the experimental results, so the established CFD model is reliable.

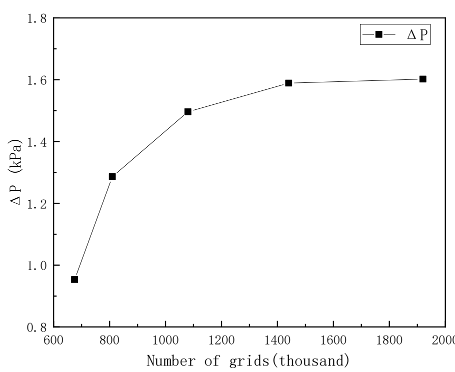


Fig. 2 Variation of pressure drop with the number of grids

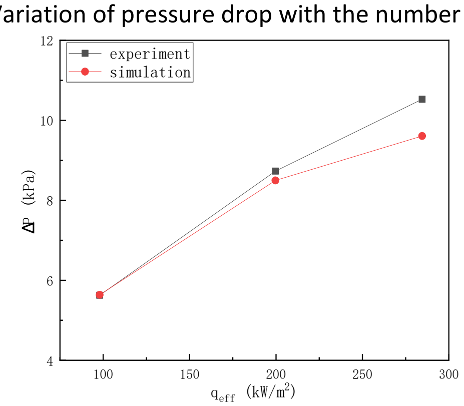


Fig. 3 Comparison between numerical and experimental data

### *2.6 Simulation cases*

Before the unsteady heat flux, it is necessary to provide an initial condition for the steady flow boiling condition. In the simulation, the initial condition are: inlet temperature of 50 ºC, the inlet mass velocity of 668.95kg/m$^2$s, and the heat flux of 338.64kW/m$^2$. When the simulation reaches the thermal equilibrium state, it's used as the steady-state flow boiling condition. At 0.068 s, after the flow condition inside the channel reaches to a stable status, the heat flux was increased instantly to the high level to simulate the effect of unsteady heat flux. The simulation cases of the unsteady state numerical calculation of flow boiling under different heat flux increases are shown in Table 1.

Table 1 Simulation cases

| Inlet temperature (ºC) | Mass velocity (kg/m$^2$s) | Initial heat flux (kW/m$^2$) | Heat flux increase (kW/m$^2$) |
|---|---|---|---|
| 50 | 668.95 | 338.64 | 97.96 |
| 50 | 668.95 | 338.64 | 199.64 |
| 50 | 668.95 | 338.64 | 284.54 |
| 50 | 668.95 | 338.64 | 580.00 |

## 3. RESULTS AND ANALYSIS

### *3.1 Bubble development characteristics during unsteady heat flux*

Fig. 4 shows the change of bubbles at 50-55mm near the outlet, when the inlet temperature is 50 ℃, the inlet mass velocity is 668.95 kg/m$^2$s, and the heat flux increase is 199.64kW/m$^2$. It can be observed from Fig. 4 that at 0.068s-0.073s, the bubbles in the microchannel are mainly a small size of isolated bubbles, which moved in the flow direction. At 0.074s, a new flow of bubbles flows from the upstream of the microchannel. With the continuous absorption of heat, the bubble size continued to increase during the flow. The aggregation of bubbles was observed at 0.081s, and a number of small bubbles attached to the side wall merged together to form a larger bubble. As more bubbles increased and aggregated, at 0.098s, the microchannel begins to form restricted bubble flow, and the volume of the bubble is restricted by the size of the channel to expand forward and backward, resulting to unstable flow. With the increase in temperature caused by the accumulation of heat, the number of restricted bubble flows in the microchannel increases, and flows out of the microchannel with the flow direction.

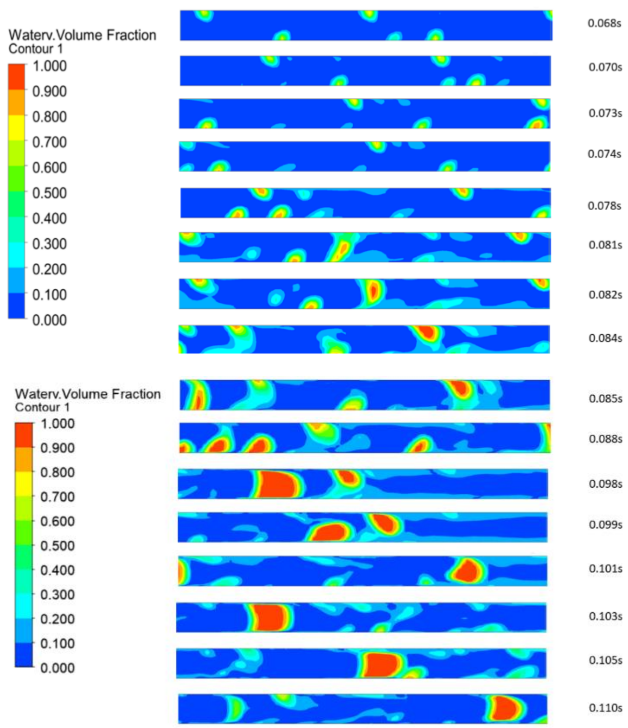


Fig. 4 When the heat flux increase is 199.64kW/m$^2$, the change of the bubble with time at a distance of 50-55mm from the inlet

### 3.2 *Influence of different heat flux increases on pressure drop characteristics*

Fig.5 shows the change of pressure drop with time under different heat flux increases: 97.96kW/m$^2$, 199.64kW/m$^2$, and 284.54 kW/m$^2$, respectively. It was found that the pressure drop first reaches a steady state when the heat flux increase is 97.96 kW/m$^2$, which was followed by heat flux increase of 199.64 kW/m$^2$, and 284.54 kW/m$^2$. Among them, the maximum value of pressure drop increase is observed at the heat flux increase of 284.54 kW/m$^2$, which is 6337.61 Pa. And the minimum pressure drop increase is observed at the heat flux increase of 97.96 kW/m$^2$, which is 2092.84 Pa. When the heat flux increase is 97.96 kW/m$^2$, the heat flux increase is the smallest. Meanwhile, the wall temperature of the microchannel reaches equilibrium, firstly. Hence, the temperature of deionized water in the microchannel will be equilibrated, firstly. Since the heat flux increase is relatively small, the temperature rise of the microchannel wall is relatively lowest, the temperature increase of deionized water in the microchannel is the smallest, and the volume fraction of water vapor is the smallest. At the same time, the bubbles are mainly comprised of isolated bubble flow and a small amount of restricted bubble flow, and the formation position of bubbles is relatively backward. Therefore, the bubbles in the microchannel are relatively small, which has relatively little influence on the pressure drop, and thus the pressure drop increase is relatively small. When the heat flux increase is 199.64 kW/m$^2$, the bubbles are mainly comprised of isolated bubble flow and restricted bubble flow, which have a great influence on pressure drop. When the heat flux increase is 284.54kW/m$^2$, the bubble is mainly comprised of annular slug flow, which has the deepest influence on pressure drop. Hence, the increase of pressure drop reaches maximum.

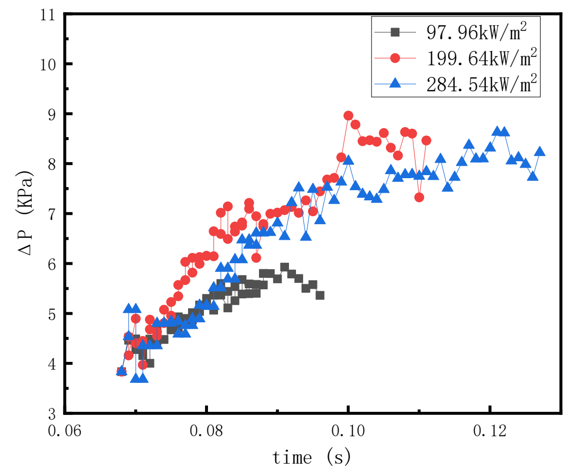


Fig. 5 Changes in pressure drop with time under different heat flux increases

### 3.3 *Influence of different heat flux increases on bubble development at the outlet of channel*

Fig. 6 shows the variation of the bubble at a distance of 50-55mm from the inlet at 0.102s under different heat flux increases. The heat flux increases were 97.96kW/m$^2$, 199.64kW/m$^2$, and 284.54 kW/m$^2$, respectively. As seen, when the heat flux increase is 97.96 kW/m$^2$, the bubbles in the microchannel are mainly isolated bubbles, and the bubble size is much smaller than the channel size. When the heat flux increase is increased to 199.64 kW/m$^2$, the bubbles in the microchannel are mainly comprised of large bubble flow and contains a small amount of restricted bubble flow. At the same time, the appearance of restricted bubble flow will give rise to the instability of flow boiling. When the heat flux increase is 284.54 kW/m$^2$, the bubbles in the microchannel are mainly annular plug flow. Meanwhile, the instability in the microchannel is intense due to the large blocking zone of the annular plug flow. When the heat flux increase is 580.00kW/m$^2$, the fluid in the microchannel is mainly the gas phase. At the same time, drying occurs in the microchannel, which leads to the reflow, and the flow boiling instability is the strongest in the microchannel. It is because the water in the microchannel absorbs more heat and produces more bubbles when the heat flux increases rise sharply. With the rise of heat flux increases, the pattern of bubble flow, is in order as follows isolated bubble flow, restricted bubble flow, and annular plug flow. As the heat flux increases continued to increase, the gas phase in the microchannel increases gradually, and the isolated bubble flow, the restricted bubble flow, the annular slug flow, and local dryness appear successively in the microchannel. As the restricted bubble flow appears, it was seen as the onset of flow boiling instability (OFI). Meanwhile, the appearance of annular plug flow leads to the increase of the instability of flow boiling, and the emergence of local dryness makes the instability of flow boiling reach the maximum.

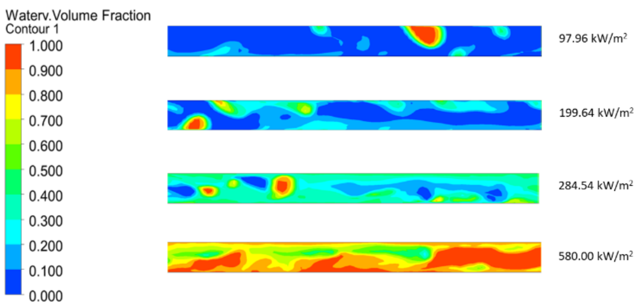

Fig. 6 Two-phase flow pattern at the bottom of microchannel at positions of 50-55mm from the inlet under different heat flux increases (*t*=0.102s)

It can be observed from Fig. 7 that there is a flow of bubbles in the microchannel before the microchannel is 9.7mm. Between 9.7mm-29.1mm, the gas phase in the microchannel increases, and the bubble flow increases. Between 29.1-38.8mm, there is mainly an annular plug flow in the microchannel. After 38.8mm, the phenomenon of local dry-out appeared in the microchannel, and when it was between 48.5mm-58mm, the phenomenon of dry-out increased. This is because the cooling medium continuously absorbs the heat transferred from the heating wall during the flow from the channel entrance to the exit during the flow and boiling process of the microchannel, and the cooling medium absorbs more and more heat along the flow direction, so as The gas phase is relatively increased in the direction of flow. The increase in heat flux density of 199.64kW/m$^2$ is relatively small compared to when the increase in heat flux density is 580.00kW/m$^2$ in the gas phase, and when the increase in heat flux density is 199.64kW/m$^2$, there are fewer restricted bubble flows in the microchannel, and the flow is boiling. The instability is small. When the heat flow density increase is 580.00kW/m$^2$, local drying occurs in the microchannel, and the flow boiling is unstable.

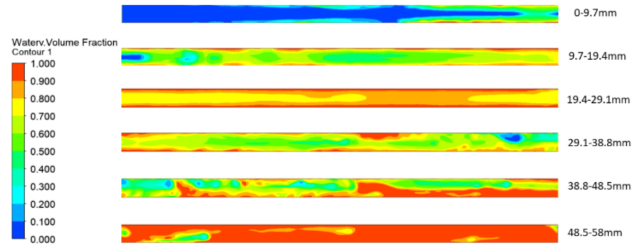

Fig. 7 Two-phase flow pattern along the channel (heat flux increase: 580.00kW/m$^2$, t= 0.102s)

### *3.4 Influence of different heat flux increases on bubble development at the outlet of channel*

Fig. 8 shows the change of the gas volume fraction on the bottom surface of the microchannel with time under different heat flux increase. It can be seen from Fig. 8 that under the same increase in heat flux density, the gas volume fraction continues to increase until it stabilizes with the sudden increase in heat flux density. Comparing the increase of different heat flux density, the relatively larger increase of heat flux has a larger gas phase volume fraction, faster growth, and greater instability. For example, when the increase in heat flux density is 284.54 kW/m$^2$, the maximum gas phase volume fraction is 0.425. At 0.068s-0.110s, the dryness basically increased by 3.5 times, an increase of 0.144; at 0.110s-0.126s, the dryness basically increased by 15.4 times, an increase of 0.250. When the heat flux density increase is 97.96 kW/m2, the maximum gas phase volume fraction is 0.104. At 0.068s-0.117s, the gas phase volume fraction increases by 1.5 times, an increase of 0.072. As the heat flow density increases, the water in the microchannel continuously absorbs heat to generate bubbles. With the generation and increase of bubbles, the volume fraction of the gas phase in the microchannel gradually increases, and the instability increases. With the increase of the heat flux density, the water in the microchannel absorbs more heat and produces relatively more bubbles, so the gas phase volume fraction is greater and the instability is greater.

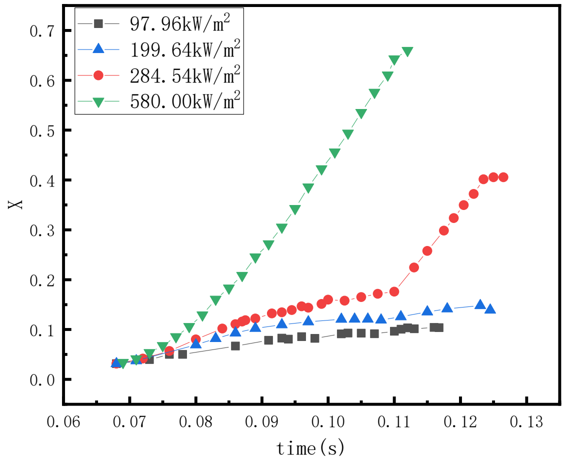

Fig. 8 Gas volume fraction of the bottom surface of the microchannel

## 4. CONCLUSIONS

By comparing the gas volume fraction diagrams of different heat flux increases, it can be found that the gas volume fraction, the growth rate of the heat flux increase, and the instability of flow boiling will increase gradually, with the rise of heat flux increase. For example, when the heat flux increase is 284.54 kW/m$^2$, the maximum gas volume fraction is 0.425. But, when the heat flux increase is 97.96 kW/m$^2$, the maximum gas volume fraction is only 0.104. The instability near the outlet of the microchannel is more likely to deteriorate due to the stronger phase transition and more gas phase at the outlet. When the heat flux increase is 580.00 kW/m$^2$, the maximum gas volume fraction is 0.923. And, when the heat flux increase is 97.96 kW/m$^2$, the maximum gas volume fraction is only 0.162.

During the process along the way in the tube, the gas phase at the heat flux increase of 199.64 kW/m$^2$, is relatively less compared to the gas phase at the heat flux increase of 580.00 kW/m$^2$. When the increase of heat flux is 199.64kW/m$^2$, there is less restricted bubble flow in the microchannel and the flow boiling instability is weak. And, when the increase of heat flux is 580.00kW/m$^2$, there is a local drying in the microchannel, and the instability of flow boiling is active. With the rise of heat flux increase, the gas phase in the microchannel increases, isolated bubble flow, restricted bubble flow, annular slug flow, and local drying appear successively in the microchannel, when the air bubble at a distance of 50mm-55mm from the inlet is at 0.102 seconds under different heat flux.


## ACKNOWLEDGEMENT

The study was supported by Grant-in-Aid for JSPS Fellows (21F20056) and Shandong Provincial Natural Science Foundation, China (No.: ZR2020ME170, ZR2016EEQ29).


## REFERENCE


[1] Hasan A, Sarwar J, Shah AH. Concentrated photovoltaic: A review of thermal aspects, challenges and opportunities. Renewable and Sustainable Energy Reviews. 2018; 94: 835-852

[2] Shukla A, Kant K, Sharma A, Biwole PH. Cooling methodologies of photovoltaic module for enhancing electrical efficiency: A review Sol Energy Mater Sol Cells, 160 (2017), pp. 275-286.

[3] Sohel Murshed SM, de Castro CA. A critical review of traditional and emerging techniques and fluids for electronics cooling. Renew Sust Energ Rev, 2017; 78: 821-833.

[4] Yang, K.; Zuo, C. A novel multi-layer manifold microchannel cooling system for concentrating photovoltaic cells. Energy Convers. Manag. 2015, 89, 214–221.

[5] Radwan, A.; Ahmed, M.; Ookawara, S. Performance enhancement of concentrated photovoltaic systems using a microchannel heat sink with nanofluids. Energy Convers. Manag. 2016, 119, 289–303.

[6] Siyabi IA, Shanks K, Mallick T, Sundaram S. Indoor and outdoor characterization of concentrating photovoltaic attached to multi-layered microchannel heat sink. Solar Energy 2020; 202: 55-72.

[7] Gilmore N, Timchenko V, Menictas C. Microchannel cooling of concentrator photovoltaics: A review. Renewable and Sustainable Energy Reviews 90 (2018) 1041–1059

[8] Zhuang J, Yu H, Mao N. An Experimental Study on Effects of Steady and Unsteady Heat Flux on Flow Boiling in Straight Microchannel. Applied Energy Symposium 2020: Low carbon cities and urban energy systems. Tokyo/Virtual, October 10-17, 2020.